Publisher: GSA
Journal: GEOL: Geology
Article ID: G35629

Anatomy of an active submarine volcano

A.F. Arnulf[1], A.J. Harding[1], G.M. Kent[2], S.M. Carbotte[3], J.P. Canales[4], and M.R. Nedimović[3,5]

[1] *Cecil H. and Ida M. Green Institute of Geophysics and Planetary Physics, Scripps Institution of Oceanography, University of California San Diego, La Jolla, California 92093, USA*

[2] *Nevada Seismological Laboratory/0174, University of Nevada, Reno, Reno, Nevada 89557, USA*

[3] *Lamont-Doherty Earth Observatory, Columbia University, Palisades, New York 10964, USA*

[4] *Department of Geology and Geophysics, Woods Hole Oceanographic Institution, Woods Hole, Massachusetts 02540, USA*

[5] *Department of Earth Sciences, Dalhousie University, Halifax, Nova Scotia B3H4J1, Canada*

ABSTRACT

Most of the magma erupted at mid-ocean ridges is stored in a mid-crustal melt lens that lies at the boundary between sheeted dikes and gabbros. Nevertheless, images of the magma pathways linking this melt lens to the overlying eruption site have remained elusive. Here, we have used seismic methods to image the thickest magma reservoir observed beneath any spreading center to date, which is principally attributed to the juxtaposition of the Juan de Fuca Ridge with the Cobb hotspot. Our results reveal a complex melt body beneath the summit caldera, which is ~14 km long, 3 km wide and up to 1 km thick. The estimated volume of the reservoir is 18–30 km^3, more than two orders of magnitude greater than the erupted magma volumes of the 1998 and 2011 eruptions. Our images show a network of sub-horizontal to shallow dipping (<30°) features that we interpret as pathways facilitating melt transport from the magma reservoir to the eruption sites.

INTRODUCTION

Axial volcano is located at the intersection of the Juan de Fuca Ridge (JdFR) and the Cobb-Eickelberg seamount chain (Fig. 1) and presents a warmer axial regime (Hooft and Detrick, 1995; Carbotte et al., 2008) and an increased crustal production rate (Hooft and Detrick, 1995, West et al., 2003). It is the most recent eruptive center of the hotspot chain (Chadwick et al., 2005), which last erupted in 2011 (Caress et al., 2012; Chadwick et al., 2012; Dziak et al., 2012). The volcano rises ~700 m above the adjacent ridge axis, has two major rift zones extending to the north and south and its summit features an 8-km-long, horseshoe-shaped caldera, where hydrothermal fields are located (Embley et al., 1990) adjacent to recent lava flows (Caress et al., 2012). Axial volcano has been the site of numerous scientific expeditions spanning nearly three decades (Crane et al., 1985; Chadwick et al., 2012), with an uptick in studies since the late 1990s prompted by its strong and quasi-cyclic volcanic activity. All these investigations have enhanced our knowledge of the geology and dynamics of Axial volcano (e.g., Caress et al., 2012; Nooner and Chadwick, 2009), but little is known concerning its internal structure.

To date, seismic experiments have been one of the keys in our understanding of the internal structure of volcanic systems (Okubo et al., 1997; Kent et al., 2000; Zandomeneghi et al., 2009; Paulatto et al., 2012). However, most experiments, especially sub-aerial-based, are restricted to refraction geometries with limited numbers of sources and receivers, and employ smoothing constraints required by tomographic inversions that are set to produce minimum velocity structure images with spatial resolutions well below the length scale of important features that define these magmatic systems (Lees, 2007). A first attempt at investigating the inner structure of Axial volcano used 5,025 airgun shots to an array of 6 ocean bottom seismometers (OBSs) and uncovered the outlines of a large crustal magma reservoir (~250 km^3), containing up to 5–21 km^3 of melt, with maximal lateral extensions of 8 by 12 km and a thickness of ~2.5 km (West et al., 2001). Though encouraging, these results were limited to first order features of the magmatic system, and the survey geometry precluded robust imaging beneath the eastern sector of the volcano.

DATA AND METHODS

In this study, we present new observations on the magmatic system of Axial volcano from four multichannel seismic (MCS) lines. These data are from the 2002 EW0207 experiment (Carbotte et al., 2006) and were acquired using a 6-km-long, 480-channel digital streamer with 12.5 m receiver intervals. The source was fired each 37.5 m and consisted of a 49.2 L airgun array.

To image the detailed geometry of the magmatic system beneath Axial volcano we followed a strategy consisting of the following steps (additional information in: Data Analysis – supplementary material): (1) the MCS data were first downward continued to the seafloor (Arnulf et al., 2014a). This process unwraps the layer 2A/2B triplication, moving the refracted energy in front of the seafloor reflection, providing information about near surface velocities. (2) A high-resolution velocity model was then obtained by performing elastic full waveform inversion (FWI) (Arnulf et al., 2012; 2014b) focused on energy arriving ahead of the seafloor reflection. The strength of FWI is that it can use the full seismic wavefield to create high-resolution velocity image of the crust, which can be used for geological interpretation. (3) The FWI velocity models were then used to create reflection images using the surface MCS data and a prestack depth reverse time migration (RTM) algorithm (Baysal et al., 1983). The advantage of RTM imaging compared to standard migration techniques is that it has no dip limitation and it handles extreme lateral velocity variations using all possible arrivals. (4) Finally, the reflectivity and seismic energy attributes of the RTM images were used to delineate the geometry (lateral extent and thickness) of the melt body, as well as other upper crustal structural features (Fig. 2; supplementary Fig. S1).

Beneath Axial volcano, our velocity models (Fig. 2A, B; supplementary Fig. S1A, B) constrain the fine-scale architecture of the shallow volcanic complex down to the top of the magma reservoir. Within this reservoir, the velocity structure is not fully constrained (and its presumed low velocity is overestimated) because the FWI, as implemented, is restricted to seismic events that have been isolated ahead of the seafloor reflection in data downward continued to a level ~1.5 km below the sea surface. In this volcanic setting, the maximum penetration of layer 2A/2B refraction event recorded on a 6-km-long streamer is ~1.25 km. Any changes in velocities below this level are manifested primarily in amplitude variation with offset (AVO) patterns of the magma chamber reflections, but these patterns are mainly sensitive to the

impedance contrast at the reflection point (Gauthier et al., 1986) and do not fully constrain the large scale background velocity. Nonetheless, the high resolution and fidelity of the FWI models of the upper ~1.5 km, which capture the largest velocity variations, allow the creation of geometrically accurate RTM images of the deeper magmatic system (Figs. 2 and 3; supplementary Figs. S1 and S2).

RESULTS AND DISCUSSION

Geometry of magma reservoir beneath Axial volcano

Our RTM images (Figs. 2 and 3; supplementary Fig. S1C and D) reveal a geometrically complex magma reservoir underlying the caldera and extending across the southeast flank of Axial volcano in a region previously thought to be devoid of significant amounts of melt (West et al., 2001). MCS profiling outlines a magma body that is at least 14 km long and 3 km wide. In places, a pair of vertically offset strong reflections is imaged, that is interpreted as top and bottom reflections from a stacked, magma sill complex as weaker reflection arrivals are seen in between. The maximum thickness of the complex is 0.6–1 km with the lower value corresponding to a pure melt case (Supplementary Fig S3). This is an order of magnitude thicker than magma reservoirs commonly found at mid ocean ridge spreading centers (Singh et al., 1998). The depth between the seafloor and the top of the magma reservoir varies between 1.1 and 2.3 km, with the two shallowest portions bounding the south rift hydrothermal field (Embley et al., 1990) and the eruptive centers of the 1998 and 2011 events (Figs. 2 and 3). On the other hand, right below the south rift hydrothermal field, the magma reservoir locally deepens, which might be related to enhanced hydrothermal cooling (Figs. 2 and 3). Interestingly, the amplitude of the magma reflector (Fig. 2E, F; supplementary Fig. S1C and D) is stronger to the southeast of the caldera, between 0 and 5 km off axis, which might reflect the location of melt delivery at depth from the Cobb hotspot to Axial volcano (Fig. 4).

Ideally, detailed constraints on P-, S-wave and anisotropic velocity structures are needed to determine the physical properties of magma bodies (Taylor and Singh, 2002). In this experiment, however, we did not fully recover such information, but our RTM approach clearly outlines the limits of the magma reservoir, which if interpolated in three-dimensions yields a maximum volume of ~30 km^3 (Fig. 4). In a pure melt case this volume would be reduced to ~18 km^3 (Supplementary Fig. S3). To refine estimates of the total melt volume present (i.e., melt versus mush content) would require further investigations. However, high melt concentration is expected within part of this reservoir, especially the southeastern sector where the strength of the magma chamber reflection along with its AVO characteristics, and the presence of a coherent P- to S- wave conversion (PmeltS reflection), suggest both high impedance contrasts at, and negligible S-wave velocity (i.e., melt with disconnected crystals) within the top of the magma chamber (Fig. 2E, F, G supplementary Fig. S1 and S4). The significant travel-time delays (~0.5 s) of first-arrival Pg phases refracting through and below the magma reservoir in the previous OBS-experiment (West et al., 2001) also suggest high melt concentration. Most of this travel-time delay now accumulates within the smaller 18–30 km^3 reservoir imaged here as opposed to the much larger reservoir (250 km^3) estimated from the OBS study. In fact, simple estimations of a one-way vertical delay through a 0.6–1 km thick magma body could account for 0.16–0.33 s, similarly 0.06–0.1 s might be explained by the low velocity lavas present in the subsiding caldera, while the rest of this travel time delay is likely explained by 3D bathymetry effects as

well as a probable low velocity region lying beneath the magma reservoir. During the 1998 and 2011 volcanic eruptions of Axial volcano, ~0.1–0.2 km^3 of magma was removed from the summit reservoir, while an even smaller portion (~0.02–0.1 km^3) was erupted at the surface (Fox et al., 2001; Caress et al., 2012; Chadwick et al., 2012). These volumes are more than two orders of magnitude smaller than Axial volcano magma reservoir, suggesting that only a small fraction of melt is extracted during each eruptive sequence. Finally, our RTM images reveal several superimposed reflectors within the summit reservoir (Figs. 2 and 3; supplementary Fig. S2), suggesting multiple imbricated melt sills. Therefore, the presence of melt in the upper crust beneath Axial volcano is likely to be distributed in a complex system of dykes, sills and conduits.

A complex magma delivery system revealed beneath Axial volcano

To date, the conduits that connect magma chambers to eruption sites have not been directly imaged; they have been inferred either from seismicity (e.g., Sohn et al., 1998) or deformation (e.g., Bagnardi et al., 2013) that result from the intrusion of magmatic dikes. Here, our RTM images (Figs. 2–4) reveal a network of sub-horizontal to shallow dipping (<30°) reflectors located between the base of Layer 2A and a horizon defined by the magma reservoir depth. These reflectors accurately tie at profile intersections (Figs. 3 and 4), and we suggest that they may be related to planes of weakness more susceptible to failure. In fact, it is likely that magmatic dikes are intruded at Axial volcano more frequently than expected from normal seafloor spreading, which may lead to formation of décollement faulting or decoupling surfaces (Amelung et al., 2007). In addition, at magma reservoir depth, a region defined by sub-horizontal reflectors of slightly higher reflectivity is imaged (Fig. 2; supplementary Figs. S1) and might mark the 50–100 m thick "crush zone" that lies within the dike-gabbroic complex transition (Agar and Klitgord, 1995). Along seismic line 63 (Figs. 2 and 4), this transitional region also connects the main magma reservoir with a secondary reservoir located ~5 km to the east and might define a preferential pathway to propagate melt away from the main reservoir and possibly along the south rift zone as suggested by the extent of the 1998 diking episode (Dziak and Fox, 1999). Finally and most interestingly, the shallowest points of the magma reservoir appear to be connected to the 1998 and 2011 eruption sites by two shallow dipping (20–30°) reflectors (Figs. 2, 3 and 4). The geometry of these reflectors is similar to circumferential intrusions (Bagnardi et al., 2013), or saucer-shaped sills (Fialko, 2001; Hansen and Cartwright, 2006) suggesting that both the 1998 and 2011 lava flows likely erupted from the same magmatic conduits in the upper crust.

CONCLUSIONS

In this study, we have applied an accurate solution for imaging an active volcano combining FWI with RTM imaging. Our approach produces velocity models of the magmatic system at Axial volcano with spatial resolutions on the order of 50–100 m. In addition, RTM imaging provide reflectivity images with spatial resolution of tens of meters. We show the clearest example to date of an unambiguous basal reflector from a melt lens system beneath a spreading center. We find that the magma reservoir is up to 1 km thick, the thickest magma reservoir observed beneath a spreading center to date, which is principally attributed to the juxtaposition of the Juan de Fuca Ridge with the Cobb hotspot. In addition, we present a unique image of the magma pathways underlying an active volcano that appears to be composed of a

network of sub-horizontal to shallow dipping faults (planes of weakness), which might cyclically be reactivated to transport melt from the magma reservoir to the eruption sites and to relieve stress build up within the volcano.

ACKNOWLEDGMENTS

This research was funded through a National Science Foundation grant, OCE-0002600, and additionally supported through the Cecil H. and Ida M. Green Foundation at the Scripps Institution of Oceanography. This study also benefited from reviews by Bill Chadwick, Jenny Collier, Páll Einarsson and Tim Wright.

REFERENCES CITED

Agar, S.M., and Klitgord, K.D., 1995, A mechanism for decoupling within the oceanic litosphere revealed in the Troodos ophiolite: Nature, v. 374, p. 232–238, doi:10.1038/374232a0.

Amelung, F., Yun, S.-H., Walter, T.R., Segall, P., and Kim, S.-W., 2007, Stress control of deep rift intrusion at Mauna Loa Volcano, Hawaii: Science, v. 316, p. 1026–1030, doi:10.1126/science.1140035.

Arnulf, A.F., Harding, A.J., Singh, S.C., Kent, G.M., and Crawford, W., 2012, Fine-scale velocity structure of upper oceanic crust from full waveform inversion of downward continued seismic reflection data at the Lucky Strike Volcano, Mid-Atlantic Ridge: Geophysical Research Letters, v. 39, L08303, doi:10.1029/2012GL051064.

Arnulf, A.F., Harding, A.J., Kent, G.M., Singh, S.C., and Crawford, W., 2014a, Constraints on the shallow velocity structure of the Lucky Strike Volcano, Mid-Atlantic Ridge, from downward continued multichannel streamer data: Journal of Geophysical Research, v. 119, doi:10.1002/2013JB010500.

Arnulf, A.F., Harding, A.J., Singh, S.C., Kent, G.M., and Crawford, W., 2014b, Nature of upper crust beneath the Lucky Strike volcano using elastic full waveform inversion of streamer data: Geophysical Journal International, v. 196, p. 1471–1491, doi:10.1093/gji/ggt461.

Bagnardi, M., Amelung, F., and Poland, M. P., 2013, A new model for the growth of basaltic shields based on deformation of Fernandina volcano, Galápagos islands, v. 377-378, p. 358-366, doi:10.1016/j.epsl.2013.07.016.

Baysal, E., Kosloff, D.D., and Sherwood, J.W.C., 1983, Reverse time migration: Geophysics, v. 48, p. 1514–1524, doi:10.1190/1.1441434.

Carbotte, S.M., Detrick, R.S., Harding, A.J., Canales, J.P., Babcock, J., Kent, G.M., van Ark, E., Nedimović, M.R., and Diebold, J.B., 2006, Rift topography linked to magmatism at the intermediate spreading Juan de Fuca Ridge: Geology, v. 34, no. 3, p. 209–212, doi:10.1130/G21969.1.

Carbotte, S.M., Nedimović, M.R., Canales, J.P., Kent, G.M., Harding, A.J., and Marjanović, M., 2008, Variable crustal structure along the Juan de Fuca Ridge: Influence of on-axis hot spots and absolute plate motions: Geochemistry Geophysics Geosystems, v. 9, no. 8, Q08001, doi:10.1029/2007GC001922.

Caress, D.W., Clague, D.A., Paduan, J.B., Martin, J.F., Dreyer, B.M., Chadwick , W.W., Jr, Denny, A., and Kelley, D.S., 2012, Repeat bathymetric surveys at 1-metre resolution of lava flows erupted at Axial Seamount in April 2011: Nature Geoscience, v. 5, p. 483–488, doi:10.1038/ngeo1496.

Chadwick, J., Perfit, M., Ridley, I., Jonasson, I., Kamenov, G., Chadwick, W., Embley, R., le Roux, P., and Smith, M., 2005, Magmatic effects of the Cobb hot spot on the Juan de Fuca Ridge: Journal of Geophysical Research, v. 110, B03101, doi:10.1029/2003JB002767.

Chadwick, W.W., Nooner, S.L., Butterfield, D.A., and Lilley, M.D., 2012, Seafloor deformation and forecasts of the April 2011 eruption at Axial Seamount: Nature Geoscience, v. 5, p. 474–477, doi:10.1038/ngeo1464.

Crane, K., Aikman, F., III, Embley, R., Hammond, S., Malahoff, A., Lupton, J., 1985, The distribution of geothermal fields on the Juan de Fuca ridge: Journal of Geophysical Research, v. 90, B1, p. 727–744, doi:10.1029/JB090iB01p00727.

Dziak, R.P., and Fox, C.G., 1999, The January 1998 Earthquake swarm at Axial Volcano, Juan de Fuca Ridge: Hydroacoustic evidence of seafloor volcanic activity: Geophysical Research Letters, v. 26, no. 23, p. 3429–3432, doi:10.1029/1999GL002332.

Dziak, R.P., Haxel, J.H., Bohnenstiehl, D.R, Chadwick, W.W., Jr, Nooner, S.L., Fowler, M.J., Matsumoto, H., Butterfield, D.A., 2012, Seismic precursors and magma ascent before the April 2011 eruption at Axial Seamount: Nature Geoscience, v. 5, p. 478–482, doi:10.1038/ngeo1490.

Embley, R.W., Murphy, K.M., and Fox, C.G., 1990, High-resolution studies of the summit of Axial Volcano: Journal of Geophysical Research, v. 95, B8, p. 12785–12812, doi:10.1029/JB095iB08p12785.

Fialko, Y., 2001, On origin of near-axis volcanism and faulting at fast spreading mid-ocean ridges: Earth and Planetary Science Letters, v. 190, p. 31–39, doi:10.1016/S0012-821X(01)00376-4.

Fox, C.G., Chadwick, W.W., and Embley, R.W., 2001, Direct observation of a submarine volcanic eruption from a sea-floor instrument caught in a lava flow: Nature, v. 412, p. 727–729, doi:10.1038/35089066.

Gauthier, O., Virieux, J., and Tarantola, A., 1986, Two-dimensional nonlinear inversion of seismic waveforms: Numerical results: Geophysics, v. 51, no. 7, p. 1387–1403, doi:10.1190/1.1442188.

Hansen, D.M., and Cartwright, J., 2006, Saucer-shaped sill with lobate morphology revealed by 3D seismic data: Implications for resolving a shallow-level sill emplacement mechanism: Journal of the Geological Society, v. 163, p. 509–523, doi:10.1144/0016-764905-073.

Hooft, E.E.E., and Detrick, R.S., 1995, Relationship between axial morphology, crustal thickness, and mantle temperature along the Juan de Fuca and Gorda Ridges: Journal of Geophysical Research, v. 100, B11, p. 22499–22508, doi:10.1029/95JB02502.

Kent, G.M., Singh, S.C., Harding, A.J., Sinha, M.C., Orcutt, J.A., Barton, P.J., White, R.S., Bazin, S., Hobbs, R.W., Tong, C.H., and Pye, J.W., 2000, Evidence from three-dimensional seismic reflectivity images for enhanced melt supply beneath mid-ocean-ridge discontinuities: Nature, v. 406, p. 614–618, doi:10.1038/35020543.

Lees, J.M., 2007, Seismic tomography of magmatic systems: Journal of Volcanology and Geothermal Research, v. 167, p. 37–56, doi:10.1016/j.jvolgeores.2007.06.008.

Nooner, S.L., and Chadwick, W.W., 2009, Volcanic inflation measured in the caldera of Axial Seamount: Implications for magma supply and future eruptions: Geochemistry Geophysics Geosystems, v. 10, no. 2, Q02002, doi:10.1029/2008GC002315.

Okubo, P.G., Benz, H.M., and Chouet, B.A., 1997, Imaging the crustal magma sources beneath Mauna Loa and Kilauea volcanoes, Hawaii: Geology, v. 25, p. 867–870, doi:10.1130/0091-7613(1997)025<0867:ITCMSB>2.3.CO;2.

Paulatto, M., Annen, C., Henstock, T.J., Kiddle, E., Minshull, T.A., Sparks, R.S.J., and Voight, B., 2012, Magma chamber properties from integrated seismic tomography and thermal modeling at Montserrat: Geochemistry Geophysics Geosystems, v. 13, no. 1, Q01014, doi:10.1029/2011GC003892.

Singh, S.C., Kent, G.M., Collier, J.S., Harding, A.J., and Orcutt, J.A., 1998, Melt to mush variations in crustal magma properties along the ridge crest at the southern East Pacific Rise: Nature, v. 394, p. 874–878, doi:10.1038/29740.

Sohn, R.A., Hildebrand, J.A., and Webb, S.C., 1998, Postrifting seismicity and a model for the 1993 diking event on the CoAxial segment, Juan de Fuca Ridge: Journal of Geophysical Research, v. 103, B5, p. 9867–9877, doi:10.1029/98JB00391.

Taylor, M.A., and Singh, S.C., 2002, Composition and microstructure of magma bodies from effective medium theory: Geophysical Journal International, v. 149, p. 15–21, doi:10.1046/j.1365-246X.2002.01577.x.

West, M., Menke, W., Tolstoy, M., Webb, S., and Sohn, R., 2001, Magma storage beneath Axial volcano on the Juan de Fuca mid-ocean ridge: Nature, v. 413, p. 833–836, doi:10.1038/35101581.

West, M., Menke, W., and Tolstoy, M., 2003, Focused magma supply at the intersection of the Cobb hotspot and the Juan de Fuca ridge: Geophysical Research Letters, v. 30, p. 1724, doi:10.1029/2003GL017104.

Zandomeneghi, D., Barclay, A., Almendros, J., Ibañez Godoy, J.M., Wilcock, W.S.D., and Ben-Zvi, T., 2009, Crustal structure of Deception Island volcano from P wave seismic tomography: Tectonic and volcanic implications: Journal of Geophysical Research, v. 114, B06310, doi:10.1029/2008JB006119.

FIGURE CAPTIONS

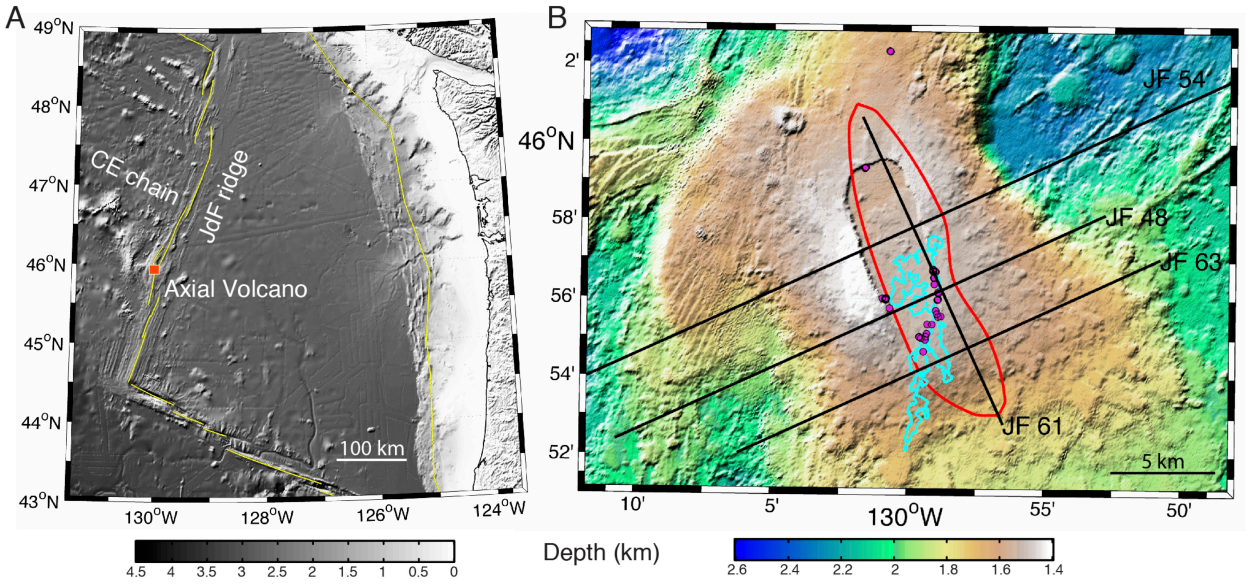

Figure 1. Bathymetry of Axial volcano. A: Study area on the Juan de Fuca (JdF) ridge, and seamounts from the Cobb-Eickelberg (CE) chain. Yellow lines outline the contour of the JdF plate. B: Analyzed seismic profiles (black lines) superimposed on a bathymetric map of Axial volcano. The cyan region marks the extent of the 2011 lava flows (Caress et al., 2012). The red

line highlights the extent of our interpreted magma body at depth. Purple hue circles mark the location of the hydrothermal vents on the seafloor.

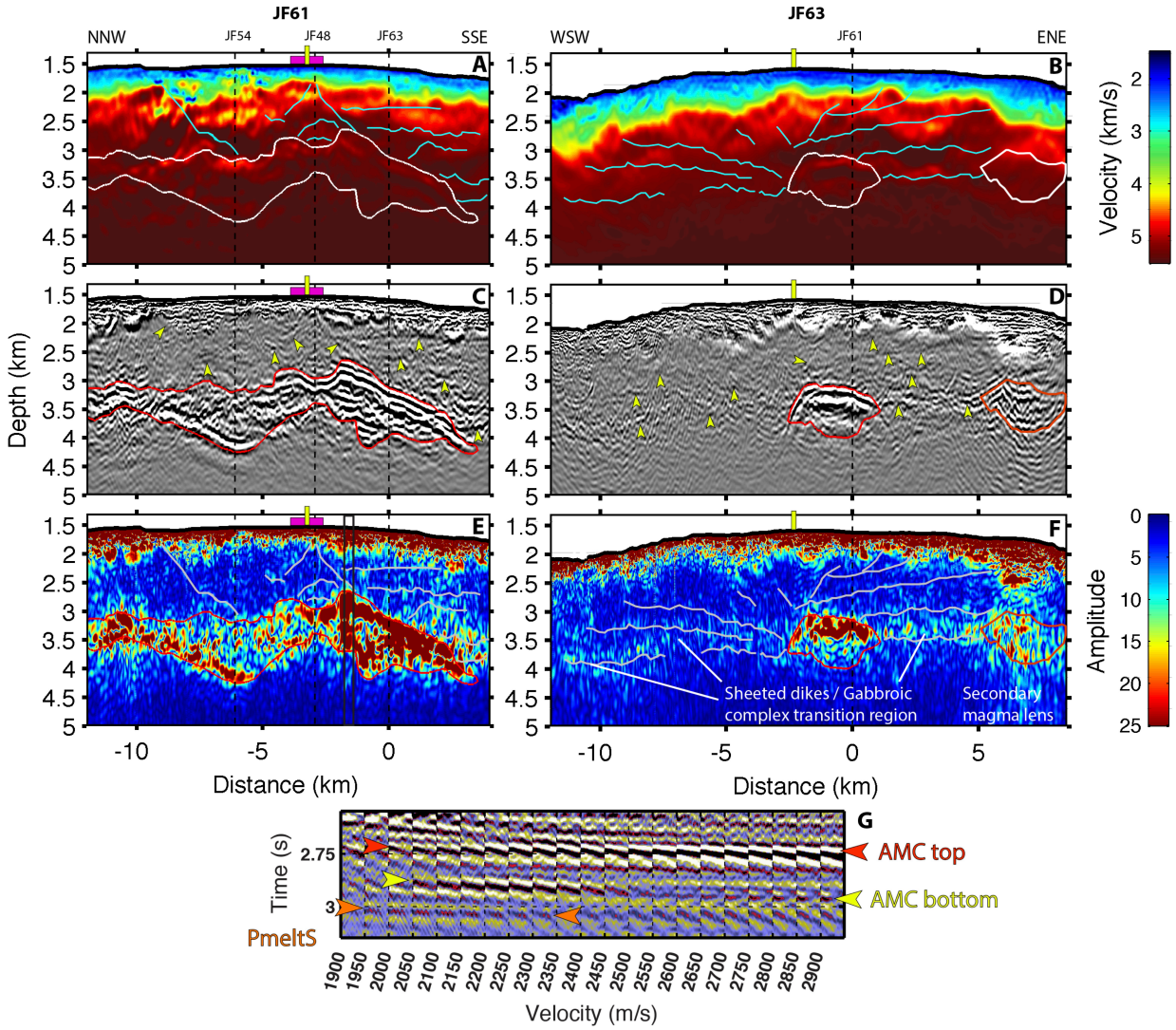

Figure 2. Upper crustal velocity, reflectivity and amplitude structure of Axial volcano along seismic lines 61 (left) and 63 (right). A, B: P-wave velocity sections. C, D: Reverse time migrated images. E, F: Amplitude envelope of the reverse time migrated images. White lines (A, B) and red lines (C, D, E and F) outline the magma reservoirs. Cyan lines (A, B), gray lines (E, F) and yellow arrows (C, D) highlight bright reflectors interpreted as planes of weakness from the RTM images, which might be activated to transport melt from the magma reservoir to the eruption sites. The vertical yellow rectangles mark the location of the south rift zone. The purple hue boxes mark the extent of the hydrothermal field along seismic line 61. The dashed vertical lines mark the intersection of the different seismic lines. G: Constant velocity stacks computed within the black rectangle along seismic line 61 (see E) are shown ranging from 1900 to 2900 m/s. Multiple events include conventional P-wave reflection from the top of the magma chamber (red arrows), as well as a complex P-wave event from the bottom of the magma chamber (yellow arrows) and a converted S-wave (PmeltS) reflection (orange arrows).

Publisher: GSA
Journal: GEOL: Geology
Article ID: G35629

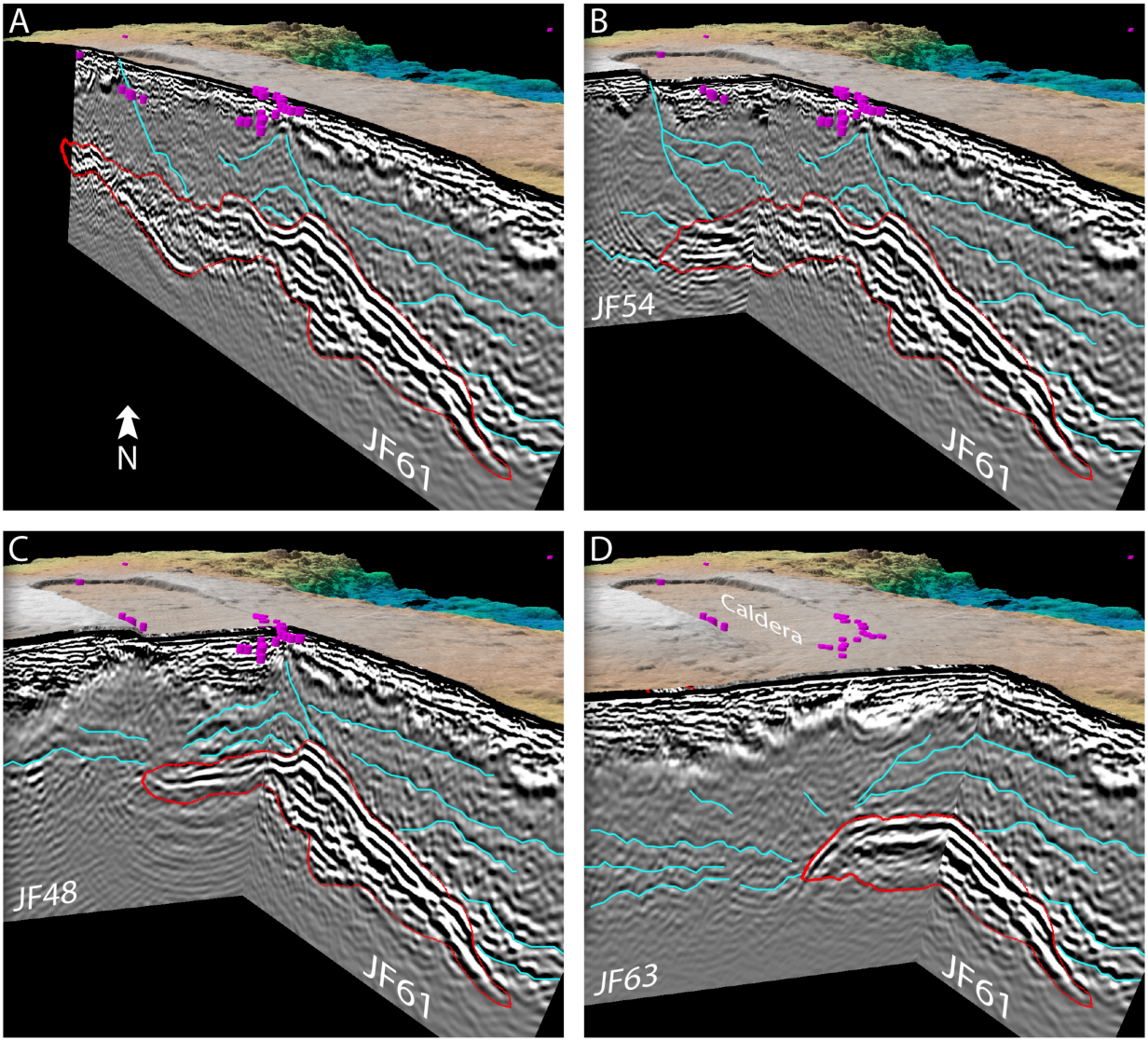

Figure 3. Perspective views of Axial volcano's magma reservoir. A: RTM image along seismic profile 61. B: Intersection of profiles 61 and 54. C: Intersection of profiles 61 and 48. D: Intersection of profiles 61 and 63. Red lines highlight the contour of the magma reservoir. Cyan lines highlight a network of sub-horizontal to shallow dipping faults that likely form the magma pathways of Axial volcano. Purple hue cylinders mark the location of the hydrothermal vents on the seafloor.

Publisher: GSA
Journal: GEOL: Geology
Article ID: G35629

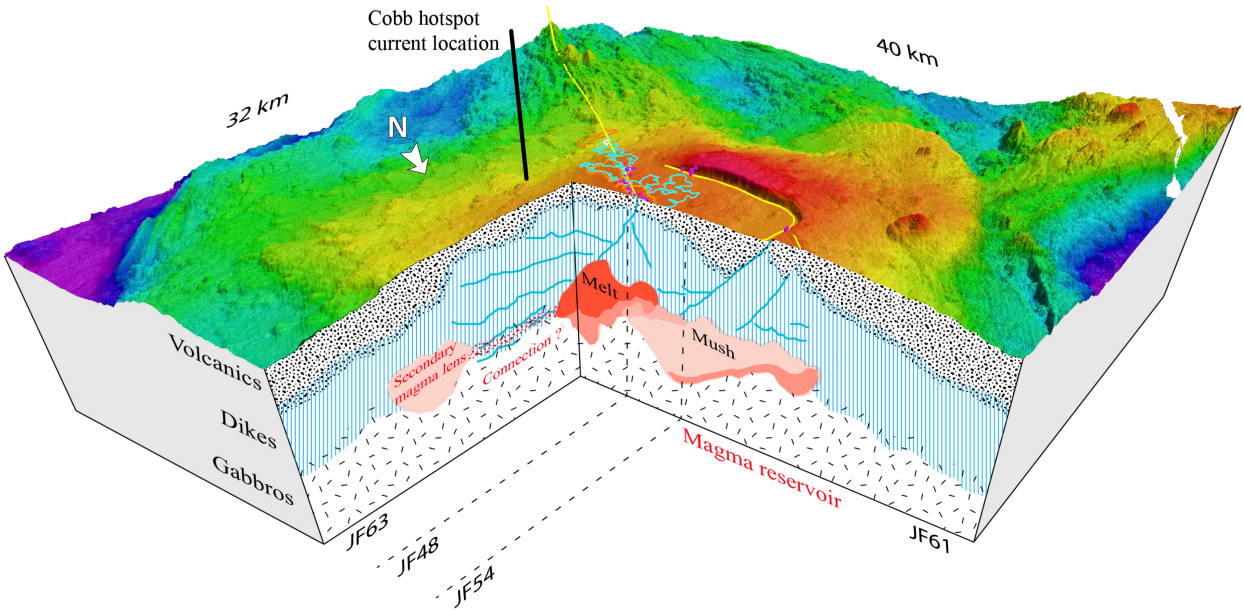

Figure 4. Schematic representation of Axial volcano magmatic system (4:1 vertical exaggeration). Axial volcano hosts the thickest magma reservoir (shades of red depending on melt content) observed beneath a spreading center to date, which is principally attributed to the juxtaposition of the Juan de Fuca Ridge with the Cobb hotspot. Several sub-horizontal to shallow dipping faults (cyan lines) might transport melt from the magma reservoir to the eruption sites and help relieve stress build up within the volcano. A secondary magma lens is located ~4 km away from the main reservoir.

[1]GSA Data Repository item 2014xxx, xxxxxxxx, is available online at www.geosociety.org/pubs/ft2014.htm, or on request from editing@geosociety.org or Documents Secretary, GSA, P.O. Box 9140, Boulder, CO 80301, USA.